A fluorescent protein-readout for transcriptional activity reveals regulation of APP nuclear signaling by phosphorylation sites

Konietzko, Uwe ; Gersbacher, Manuel T ; Streuli, Jeremy ; Krüger, Maik ; Thöni, Sarina ; Kins, Stefan ; Nitsch, Roger M

Abstract: Signaling pathways that originate at the plasma membrane, including regulated intramembrane proteolysis (RIP), enable extracellular cues to control transcription. We modified the yeast Gal4 transcription system to study the nuclear translocation of transcriptionally active complexes using the fluorescent protein citrine (Cit) as a reporter. This enabled highly sensitive quantitative analysis of transcription in situ at the single cell level. The Gal4/UAS-Cit transcription assay displayed a sigmoidal response limited by the number of integrated reporter cassettes. We validated the assay by analyzing nuclear translocation of the amyloid precursor protein (APP) intracellular domain (AICD) and confirmed the requirement of Fe65 for nuclear translocation of AICD. In addition to the strong on-off effects on transcriptional activity, the results of this assay establish that phosphorylation modifies nuclear signaling. The Y682F mutation in APP showed the strongest increase in Cit expression, underscoring its role in regulating Fe65 binding. Together, we established a highly sensitive fluorescent protein-based assay that can monitor transcriptional activity at the single cell level and demonstrate that AICD phosphorylation affects Fe65 nuclear activity. This assay also introduces a platform for future single cell-based drug screening methods for nuclear translocation.

DOI: https://doi.org/10.1515/hsz-2019-0125

Uwe Konietzko*, Manuel T. Gersbacher, Jeremy Streuli, Maik Krüger, Sarina Thöni, Stefan Kins and Roger M. Nitsch

A fluorescent protein-readout for transcriptional activity reveals regulation of APP nuclear signaling by phosphorylation sites

https://doi.org/10.1515/hsz-2019-0125
Received January 24, 2019; accepted May 14, 2019

Abstract: Signaling pathways that originate at the plasma membrane, including regulated intramembrane proteolysis (RIP), enable extracellular cues to control transcription. We modified the yeast Gal4 transcription system to study the nuclear translocation of transcriptionally active complexes using the fluorescent protein citrine (Cit) as a reporter. This enabled highly sensitive quantitative analysis of transcription in situ at the single cell level. The Gal4/UAS-Cit transcription assay displayed a sigmoidal response limited by the number of integrated reporter cassettes. We validated the assay by analyzing nuclear translocation of the amyloid precursor protein (APP) intracellular domain (AICD) and confirmed the requirement of Fe65 for nuclear translocation of AICD. In addition to the strong on-off effects on transcriptional activity, the results of this assay establish that phosphorylation modifies nuclear signaling. The Y682F mutation in APP showed the strongest increase in Cit expression, underscoring its role in regulating Fe65 binding. Together, we established a highly sensitive fluorescent protein-based assay that can monitor transcriptional activity at the single cell level and demonstrate that AICD phosphorylation affects Fe65 nuclear activity. This assay also introduces a platform for future single cell-based drug screening methods for nuclear translocation.

Keywords: amyloid precursor protein; amyloid precursor protein intracellular domain (AICD); Fe65; Gal4/UAS assay; nuclear translocation; regulated intramembrane proteolysis (RIP).

***Corresponding author: Uwe Konietzko,** Institute for Regenerative Medicine (IREM), University of Zurich, Wagistrasse 12, 8952 Schlieren, Switzerland, e-mail: uwe.konietzko@irem.uzh.ch
Manuel T. Gersbacher, Jeremy Streuli, Maik Krüger, Sarina Thöni and Roger M. Nitsch: Institute for Regenerative Medicine (IREM), University of Zurich, 8952 Schlieren, Switzerland
Stefan Kins: Division of Human Biology and Human Genetics, Technical University of Kaiserslautern (TUK), 67663 Kaiserslautern, Germany

Introduction

Regulated intramembrane proteolysis (RIP) of transmembrane proteins by the γ-secretase complex releases the intracellular domains (ICDs) from the membrane. Subsequently, these ICDs can translocate to the nucleus to activate transcription, as originally shown for RIP of the Notch receptor (De Strooper et al., 1999). Exploration of nuclear signaling is achieved by microscope analysis of nuclear translocation or subcellular fractionation of nuclei coupled to detection of the ICDs. To directly measure transcriptional activity, reporter systems consisting of promoter sequences fused to enzymes that generate measurable signals have been used. In the case of Notch, where target genes are clearly identified, endogenous promoters of the genes can be fused to reporter enzymes. Identification and characterization of transcriptional activators with unknown target sequences is often done with the yeast-derived Gal4/UAS system (Kakidani and Ptashne, 1988). Herein, the Gal4 DNA-binding domain (Gal4-DBD) is fused to a protein of interest (POI). The Gal4-DBD binds to an array of upstream activating sequences (UAS), leading to the expression of a downstream reporter gene if the POI has transcriptional activity. Frequently used reporter genes are β-galactosidase, which generates a color precipitate identifiable in a microscope, and luciferase, which can be quantified using luminescence plate readers. Fluorescent protein reporters have mainly been used to study neuron morphology and connectivity using binary systems for targeted gene expression in *Drosophila* and zebrafish, where different Gal4 driver lines are combined with a variety of different UAS-linked transgenes (Duffy, 2002; Scott, 2009).

None of the methodologies to investigate nuclear signaling is without caveat. Antibody-based detection can be difficult in the nuclei of fixed cells, due to the dense packing of DNA, RNA, and proteins (Konietzko et al., 2010). Therefore, the study of nuclear translocation often relies on fusing a fluorescent protein to the POI, which might alter its localization, metabolism, and function. When performing isolation of nuclei by subcellular fractionation, there

is inevitable contamination by the endoplasmic reticulum (ER) that is connected to the outer nuclear membrane. Thus, when studying nuclear signaling by transmembrane RIP substrates, there will be contamination by the full-length proteins that are synthesized in the ER.

Analysis of transcriptional activity with the Gal4/UAS system is usually done by transient plasmid transfection of cell lines. The need to transfect multiple plasmids (i.e. reporter constructs, Gal4-DBD-fused transcription factors, further accessory proteins) results in varying combinations of the individual plasmids in different cells. Furthermore, with transient transfection, plasmids enter the cells via endocytosis, are released into the cytosol, and are transported toward the nucleus. Nuclear entry occurs only when the nuclear membrane breaks down during mitosis, unless the plasmids harbor a DNA nuclear targeting signal (Bai et al., 2017). This is not the case for the commonly used luciferase reporter plasmids. Hence, a variable amount of transfected reporter plasmid enters the nucleus, depending on the replication rate of the cell line and the assay time post-lipofection. Furthermore, luciferase assays employ lysis of the cells, mixing the subcellular compartments for varying times before readout. Taken together, transient transfection of multiple plasmids and lysis of cells for signal detection introduces variability that can obscure modulatory influences on plasma membrane to nucleus signaling and transcriptional activity.

Here, we developed a variant Gal4-based assay using the fluorescent protein citrine (Cit) as a reporter. We introduced the reporter construct via lentiviral infection to generate cell lines with stable integration of the reporter in the genome. This ensures that the expression of Cit is regulated by bona fide nuclear translocation. After cell fixation, Cit fluorescence can be analyzed in situ without further processing. We developed the system for quantification by either confocal microscopy or plate readers. The assay was applied to study nuclear signaling by the RIP substrate amyloid precursor protein (APP).

Results

Fluorescence readout for Gal4-dependent transcriptional activity

To establish a cellular assay for transcriptional activity that enables readout using microscopy we used the fluorescent protein Cit to replace the commonly used luciferase or β-galactosidase reporters. For this, nine consecutive Gal4-binding sequences (9×UAS) were placed upstream of the Cit cDNA (Figure 1A) and cloned into a pCCL-derived third-generation lentiviral vector. This lentiviral vector was used to generate HEK293 cells that harbor stable genomic integration of the reporter construct (HEK:UAS-Cit). Transfection of reporter cells with the strong viral activator VP16 fused to a Gal4-DBD sequence (Gal4-VP16) revealed strong induction of Cit fluorescence by confocal microscopy (Figure 1B). Mock transfected reporter cells, in contrast, showed only weak fluorescence signal, indicating low reporter construct leakiness (Figure 1B). APP with a Gal4-DBD inserted internally, preceding the AICD (contributed by Tom Südhof), was used to validate our assay system. APP-Gal4 alone caused a small, but significant increase in Cit fluorescence that was strongly enhanced by Fe65 co-expression (Figure 1B). For quantification, we measured the total Cit fluorescence and normalized it to the number of DAPI-stained nuclei (Figure 1C). The transcriptional activity of APP, together with Fe65, reached approximately 15% of the activity of the strong viral activator VP16.

We observed that, in some cases, nuclei are not identified during the ImageJ analysis, i.e. when size or DAPI thresholding is outside of the set values for detection. Cit expressed by these cells will nevertheless be picked up with total Cit measurements. To enhance the accuracy of quantification, we fused three NLS to Cit, targeting it to the nucleus. Cit fluorescence was measured solely in the nucleus using the nuclear outline demarcated by DAPI staining, hence quantifying only nuclei that are counted for normalization (Figure 1D).

We infected HEK293 cells with reporter virus once (HEK1:UAS-Cit-NLS) and twice (HEK2:UAS-Cit-NLS). With the used virus titers of 10^7–10^8/ml supernatant, we assumed a 100% infection efficiency of HEK293 cells (10^5) and thus expected a maximum of approximately 100–1000 or 200–2000 integrations per cell line, respectively (see the Materials and Methods). We titrated the Gal4-VP16-expressing plasmid and saw a sigmoidal response of the Cit fluorescence signal, with the twice-infected cell line shifted to higher levels (Figure 1E). Titration of a plasmid directly expressing a nucleus-targeted fluorescent protein Cerulean (Cer)-NLS via a CMV promoter into HEK293 cells showed a non-saturated exponential increase in nuclear fluorescence over the same DNA concentration range (Figure 1F). This suggests that the Cit fluorescence signal observed with the Gal4-VP16-expression plasmid is caused by limited insertion sites of the UAS-Cit-NLS.

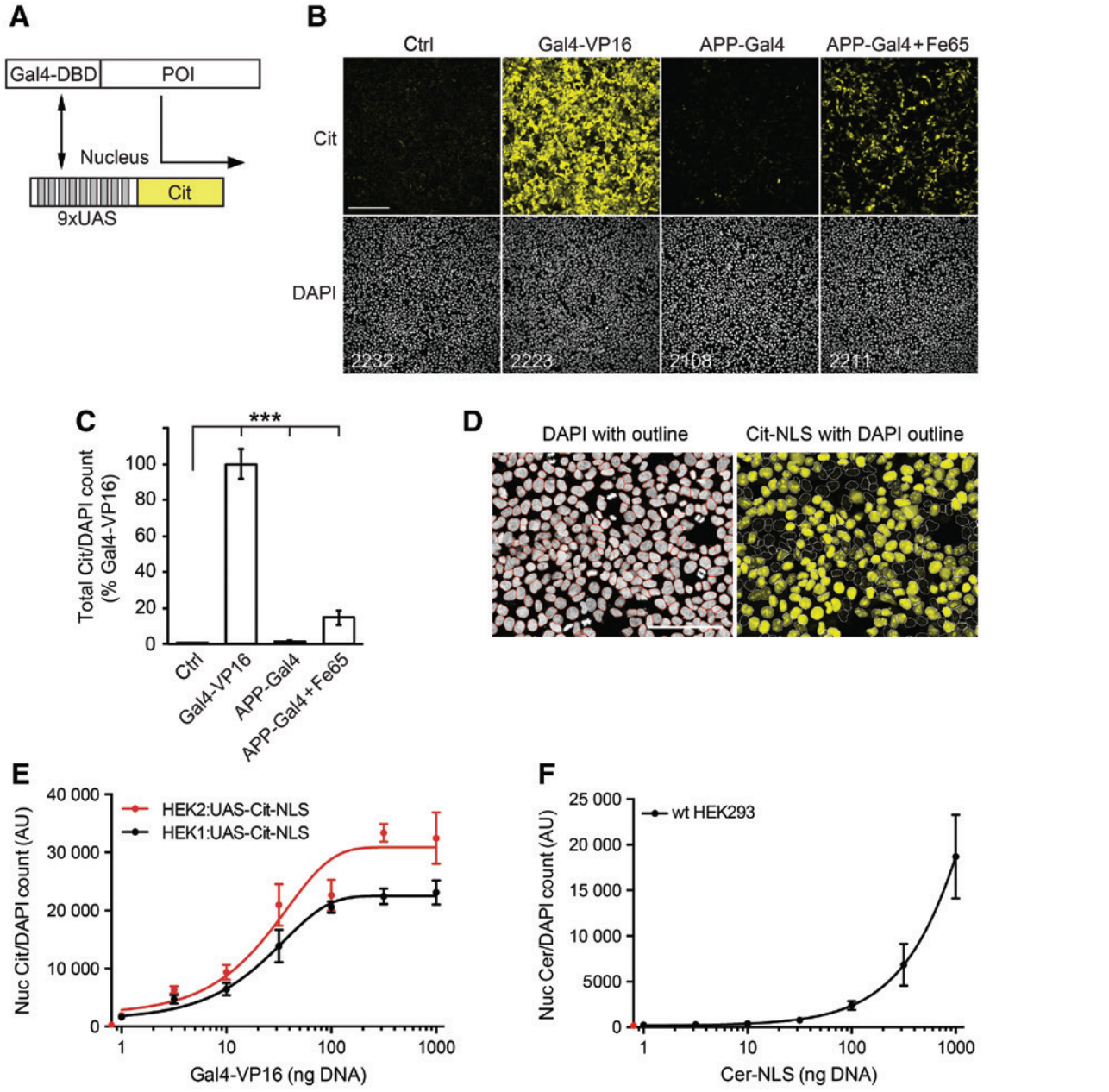

Figure 1: Fluorescence readout for Gal4-dependent transcriptional activity.
(A) Scheme of the assay principle. The DBD is fused to a POI and transfected into cell lines that harbor lentivirus-mediated genomic integrations of nine consecutive upstream Gal4-binding sequences (9×UAS), driving expression of the enhanced yellow fluorescent protein Cit. The transcriptional activity of the POI or associated proteins can be quantified by measuring Cit fluorescence. (B) Confocal microscopy images of a HEK:UAS-Cit cell line without treatment (ctrl) or transfected with Gal4-VP16, APP-Gal4, or APP-Gal4 together with Fe65. Numbers of DAPI-stained nuclei per frame are indicated. Scale bar: 200 μm. (C) Total Cit fluorescence was measured per frame and normalized to nuclei counts. Ten frames per condition were imaged from two different passages. Bars show mean ± SD. (D) Confocal microscopy images of a reporter HEK cell line expressing Cit-NLS transfected with Gal4-VP16. The DAPI-stained nuclear outline was determined with Fiji and used to measure the Cit signal solely in the nucleus. Scale bar: 100 μm. (E) DNA concentration series of Gal4-VP16 transfected into cells infected once (HEK1:UAS-Cit-NLS) or twice (HEK2:UAS-Cit-NLS) with the reporter virus expressing Cit-NLS. Quantification of nuclear Cit signal was performed on confocal microscopy images (n = 6 per concentration; shown as mean ± SD). The red dot on the y-axis denotes fluorescence of non-transfected cells. (F) DNA concentration series of Cer-NLS was transfected into wild-type HEK293 cells, and quantification was performed on confocal microscopy images (n = 6 per concentration; shown is mean ± SD). The red dot on the y-axis denotes fluorescence of non-transfected cells.

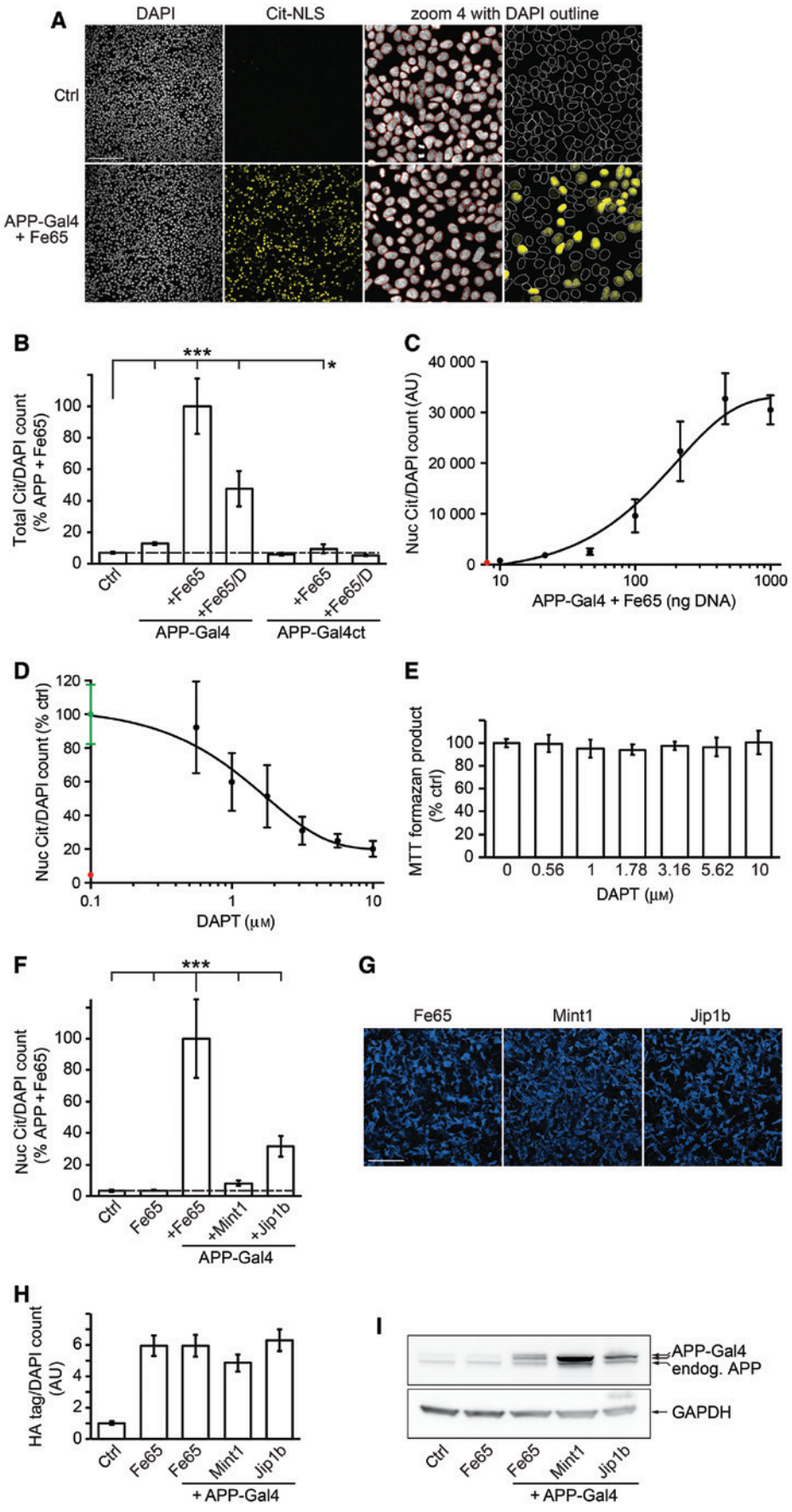

Figure 2: Characterization of APP transcriptional activity.
(A) HEK2:UAS-Cit-NLS cells transfected with APP-Gal4 and Fe65. Confocal microscopy pictures on the left show the frames imaged for quantification. On the right, a fourfold magnification from part of the images is shown with the DAPI outline determined in Fiji. Scale bar: 200 μm. (B) HEK2:UAS-Cit-NLS cells transfected with APP-Gal4 and GAL4 fusion to the C-terminus of AICD (APP-Gal4ct) with and without Fe65. Fe65 co-expressing cells were further treated with 1 μM DAPT (D). Cit fluorescence was determined with confocal microscopy. Ten frames were imaged per condition from two different passages. Bars show mean ± SD. (C) A cDNA concentration series of APP-Gal4 and Fe65 was used for transfection of HEK2:UAS-Cit-NLS cells and quantification was performed with confocal microscopy images (n = 6 frames per concentration for every of 3 passages; mean ± SD). The red dot on the y-axis denotes fluorescence of non-transfected cells. (D) Inhibition of γ-secretase with a DAPT concentration series in HEK2:UAS-Cit-NLS cells transfected with APP-Gal4 and Fe65. Quantification of nuclear Cit fluorescence shows dose-dependent inhibition (n = 6 frames per concentration for every of 3 passages; mean ± SD). The red dot on the y-axis denotes fluorescence of non-transfected cells. Green dot and SD denote the value of transfected cells without DAPT. (E) MTT assay reveals no toxicity of the DAPT concentration series. (F) Effects of different APP-interacting proteins, transfected into HEK2:UAS-Cit-NLS cells, on the transcriptional activity of APP-Gal4 quantified with confocal microscopy (n = 6 frames per lipofection for every passage of a total of 3; bars show mean ± SD). (G) Representative confocal microscope images of the experiment shown in (F) showing HA tag staining of the transfected APP-binding proteins. Scale bar: 200 μm. (H) Quantification of total fluorescence from the stained APP-binding proteins of the experiment shown in (F), normalized to the DAPI counts. (I) Western blot analysis with anti-APP antibody detecting endogenous APP and the transfected APP-Gal4. Low exposure shows only a faint band of endogenous mature APP that is superimposed by the immature and mature APP-Gal4 bands, which run higher due to the approximately 20-kDa Gal4-DBD, while endogenous immature APP can still be resolved. Increased immature APP levels were detected upon co-expression of Mint1 or Jip1b as compared to Fe65.

APP-mediated nuclear signaling using microscopic inspection

For the analysis of AICD translocation to the nucleus, we again used the HEK2:UAS-Cit-NLS cell line (Figure 2A). To ensure measurement of the signals in the linear range, we adjusted the laser intensity and photon accumulation accordingly (for details, see the Materials and Methods). We transfected the cells either with an empty vector (control) APP-Gal4 alone or together with Fe65, which caused a nearly 10-fold increase in the Cit signal (Figure 2A, B). Inhibition of APP cleavage by 1 μM DAPT (D) led to a strong reduction in the Cit signal. We also cloned an expression vector, encoding APP with a C-terminal fusion of the Gal4-DBD (APP-Gal4ct). Notably, this construct caused only minor activity over the background in the presence of Fe65. Titration of the APP-Gal4 construct together with Fe65 revealed a sigmoidal response with saturation of the reporter system at higher DNA concentrations, similar to the Gal4-VP16-induced Cit signal (Figure 2C). As inhibition of nuclear signaling by 1 μM DAPT did not completely block transactivation of the Cit reporter (Figure 2B), we analyzed a concentration series (0.56–10 μM) of DAPT inhibition. Increasing DAPT concentrations showed a dose-dependent decrease of the Cit signal with half-maximal inhibition at approximately 2 μM DAPT (Figure 2D). To exclude DAPT toxicity throughout the concentration series, we performed MTT assays, revealing no effect on cell viability (Figure 2E).

A variety of different adapter proteins have been shown to bind to AICD. We tested if other proteins, aside from Fe65, would support APP-Gal4-mediated Cit expression. Fe65 alone did not induce Cit expression because a Gal4-DBD sequence is necessary to target transcriptional activators to the reporter sequences (Figure 2F). Together with APP-Gal4, we again detected a strong expression of Cit when Fe65 is co-expressed. In contrast, Mint1/X11 co-expression did not reveal any transcriptional activation over the levels seen for APP-Gal4 alone. Co-expression of Jip1b significantly increased reporter gene expression, but to a much lower extent than that of Fe65. Equal protein abundance of HA-tagged Fe65, Mint1, and Jip1b was validated by staining the analyzed cells with anti-HA antibody and quantifying the total fluorescence (Figure 2G, H). The effect of the different adaptor proteins on APP levels was verified with Western blots (Figure 2I). Co-transfection of identical amounts of APP-Gal4 plasmid with the different APP-interacting proteins resulted in different APP levels as predicted from published data. Lowest full-length APP levels were seen with Fe65 that promotes APP turnover (Sabo et al., 1999), whereas Mint1/X11 and Jip1b, which are reported to stabilize full-length APP (Borg et al., 1998; Taru et al., 2002), increased APP levels, both of endogenous APP and transfected APP-Gal4. Co-expression of Fe65 thus resulted in lowest APP-Gal4 levels, but this adapter protein induced the strongest expression of Cit.

APP-mediated nuclear signaling using plate reader analysis

We next analyzed the Gal4/UAS-Cit transcription assay using a fluorescence plate reader. To determine fluorescence signals due to leakage expression, we calculated

the LoB (Armbruster and Pry, 2008), as described in the Materials and Methods section, and subtracted this value from those of the experimental measurements. As with the results of confocal microscopy analysis (Figure 1E), titration of a Gal4-VP16-expressing plasmid resulted in a sigmoidal response with similar dose-response relations (Figure 3A). Co-expression of APP-Gal4 and Fe65 also resulted in a dose-response relation similar to the microscopy analysis shown in Figure 2C, with saturation of the Cit signal at 300 ng of each plasmid (Figure 3B).

To determine if plate reader analysis would allow medium-throughput pharmacological screening, we established an in-suspension lipofection protocol. HEK2:UAS-Cit-NLS cells were transfected with APP-Gal4 and Fe65 in suspension and distributed onto 48-well plates to ensure homogenous cell populations in different wells. We tested a concentration series of the γ-secretase inhibitor DAPT (Figure 3C). Again, increasing DAPT concentrations showed a dose-dependent decrease of the Cit signal with half-maximal inhibition at approximately 2 μM DAPT. Together, the plate reader analysis revealed results similar to those of confocal microscopy analysis of the UAS-Cit reporter cells.

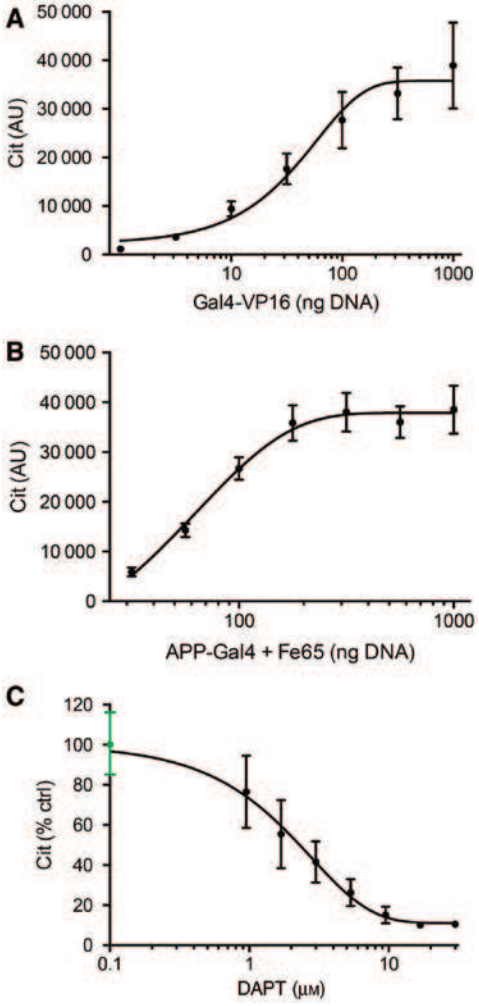

Figure 3: Plate reader analysis of transcriptional activity. (A) HEK2:UAS-Cit-NLS cells were grown in 24-well plates and transfected with a cDNA concentration series of Gal4-VP16. Fluorescent Cit signals and cell confluence measurements were acquired with a Tecan plate reader. Cit signals were normalized by cell confluence and plotted as mean ± SD. (B) Similar to A with transfection of a cDNA concentration series of APP-Gal4 and Fe65. (C) HEK2:UAS-Cit-NLS cells transfected in suspension with APP-Gal4 and Fe65 before plating on 24-well plates. Cells were treated with a DAPT concentration series for 20 h and measured with a plate reader as in A.

Regulation of APP-mediated nuclear signaling

To test the sensitivity of our assay system, we tested APP mutations affecting Fe65 binding, G681A, which disrupts the interaction, and Y682F, which prevents tyrosine phosphorylation and thus enhances Fe65 binding (Figure 4A). Compared with the co-expression of wild-type APP-Gal4 together with Fe65, G681A mutation nearly abolishes the generation of a Cit signal (Figure 4B) to levels similar to those observed with APP-GAL4 alone (Figure 2). In contrast, Y682F mutation leads to a significantly increased Cit signal. Representative confocal microscopy images are shown (Figure 4C).

We mutated several residues that have been described to be phosphorylated: serine and threonine to alanine and tyrosine to phenylalanine, to prevent phosphorylation at these sites. Initial experiments with lipofection of 1 μg of plasmid DNA did not show any difference in the Cit signal with different mutants except the G681A mutation that abolished transcriptional activity. We reduced the DNA concentration to 100 ng, which lies in the linear response range of the Gal4/UAS-Cit transcription assay. Mutation of S655 or Y687 resulted in a reduced Cit signal, whereas T668 and S675 slightly increased it (Figure 4D). The strongest increase in expression was again observed with the Y682F mutant. We performed Western blots to determine the effects of the different mutations on full-length APP (Figure 4E). The levels of immature and mature APP-Gal4 for the different phosphomutants are highly similar, except the Y687F mutant, which presented reduced levels. The G681A mutation that disrupts Fe65 binding leads to a selective reduction of the mature APP-Gal4 band.

We previously reported that mutation of the VML sequence of AICD to LLR resulted in reduced AICD levels (Gersbacher et al., 2013). Insertion of the LLR mutation into APP-Gal4 strongly reduced induction of Cit

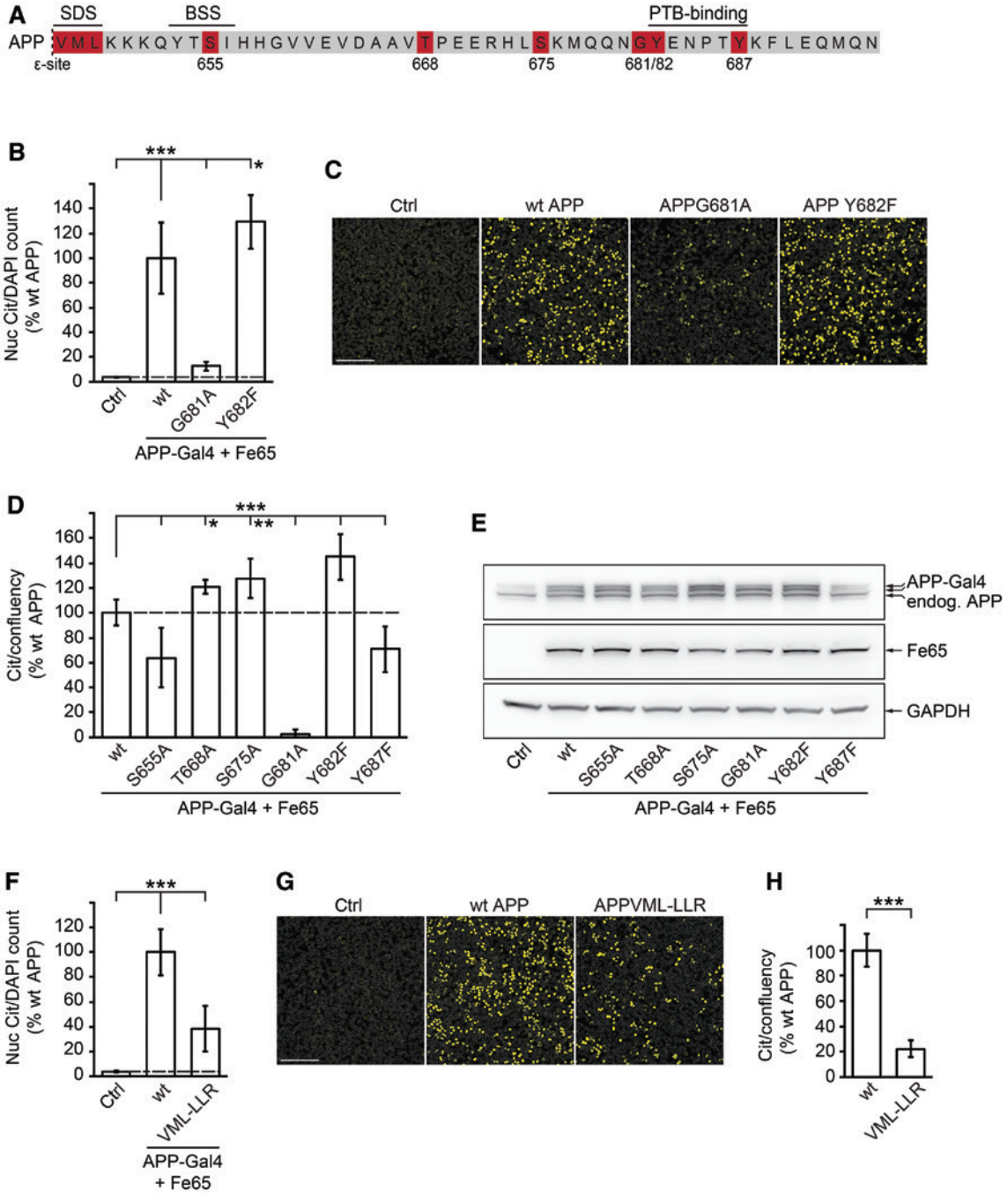

Figure 4: Mutations in AICD reveal regulation of transcriptional activity.
(A) Human AICD amino acid sequence starting from the ε-cleavage site with mutations highlighted in red. SDS: stability-determining sequence; BSS: basolateral sorting signal. PTB: PTB domain binding site. (B) Confocal microscopy analysis of HEK2:UAS-Cit-NLS cells transfected with APP G681A and Y682F mutants together with Fe65 (7 frames imaged; bars show mean ± SD). (C) Representative confocal microscopy images from the experiment shown in (B). Scale bar: 200 μm. (D) Plate reader analysis of HEK2:UAS-Cit-NLS cells expressing Fe65 and APP variants with mutation of reported phosphorylated residues (3 wells per passage of 3 in total; bars show mean ± SD). (E) Western blot analysis of different the APP-Gal4 phosphomutants analyzed in (D). Anti-APP antibody detects endogenous APP and the transfected APP-Gal4. Extracts of non-transfected HEK2:UAS-Cit-NLS (ctrl) showed signals for the immature and mature forms of endogenous APP. Signals from transfected APP-Gal4 revealed a higher apparent molecular weight, which is likely due to the approximately additional 20 kDa of the Gal4-DBD, and superimpose with the – in comparison – weak signal of endogenous mature APP. (F) Confocal microscopy analysis of HEK2:UAS-Cit-NLS cells transfected with APP VML-LLR mutant or wt together with Fe65 (n = 6 frames per clone for every passage of a total of 3; shown is mean ± SD). (G) Representative confocal microscopy images from the experiment shown in (F). Scale bar: 200 μm. (H) Plate reader analysis of HEK2:UAS-Cit-NLS cells transfected with APP VML-LLR mutant or wt together with Fe65 (3 wells per passage of 3 in total; bars show mean ± SD).

expression when analyzed by confocal microscopy or with plate reader analysis (Figure 4F, H). Representative confocal microscopy images are shown (Figure 4G). These data clearly show that our GAL4/Cit-based assay mirrors the expected results of modulating APP mutations.

Discussion

We have developed a Gal4-based assay to determine POI transcriptional activity via expression of the fluorescent protein Cit. A crucial advantage is the nuclear localization of the reporter DNA constructs that are inserted via lentiviral vectors into the genome. This ensures the detection of bona fide nuclear translocation. Further, the mutational analysis of Fe65 indicates that the assay system allows, aside from studying nuclear translocation, testing for transcription activity properties. Stable cell lines also eliminate the necessity to transfect two luciferase reporter plasmids in addition to the POIs studied, reducing variability due to non-homogenous transfection ratios of plasmids in individual cells. Furthermore, the signal can be analyzed in situ without cell lysis, allowing the staining and subcellular localization of proteins under investigation. Readout is achieved by quantifying Cit fluorescence via confocal microscopy or plate reader. With the evolved Cit-NLS reporter, confocal imaging offers accurate determination of Cit-NLS levels in nuclei demarcated by DAPI staining and thus enables analysis at the single cell level. This is of particular interest for combined analysis, studying additional cellular alterations besides nuclear translocation. We further established an in-suspension lipofection protocol to transfect cells before plating homogenous cell populations into multi-well plates. Medium-throughput drug screening is feasible, as we have shown for a dilution series of the γ-secretase inhibitor DAPT. The IC_{50} in our experiments is higher than reported values of 100–200 nM that were determined with ELISAs measuring the Aβ generated in in vitro assays using recombinant peptides and cell membranes (Dovey et al., 2001). This probably relates to the high sensitivity of our assay, in which, in living cells, a few AICD-Fe65 complexes in the nucleus are sufficient to drive the expression of many Cit molecules.

Titration of different transcriptional activators in reporter cell lines resulted in a sigmoidal increase in the Cit fluorescence signal, saturating at higher DNA concentrations. This is in contrast to the exponential increase in fluorescence when the fluorescent protein is expressed directly from a transfected plasmid. The sigmoidal response results from the limited number of reporter integrations in the nucleus that we estimated to be theoretically maximally 2000 if all virus particles would have infected the cells and integrated into the genome (see section 'Results'). Thus, as single plasmids with CMV promoter lead to expression of hundreds to thousands of transcripts, expression of Cit saturates likely with transfection of only very few or possibly a single plasmid.

APP is central to Alzheimer disease, with cleavage of this transmembrane protein by RIP generating the Aβ peptide and AICD (De Strooper and Annaert, 2000; Pardossi-Piquard and Checler, 2012). The release of AICD from the membrane is followed by nuclear translocation, together with its interacting protein Fe65 (Duilio et al., 1991; Kimberly et al., 2001). In the nucleus, AICD-Fe65 co-localizes with Tip60 in AFT spots that have properties resembling phase-separated condensates, which are involved in regulating transcription (von Rotz et al., 2004; Muller et al., 2007; Konietzko et al., 2010; Cho et al., 2018). Using Gal4-based luciferase assays, AICD, together with Fe65, was shown to have transcriptional activity (Cao and Sudhof, 2001). Our findings using the Gal4/UAS-Cit transcription assay are in line with the published results. We observe a strong dependence on Fe65 co-expression that has also been demonstrated by other groups studying AICD transcriptional activity (Zambrano et al., 2004; Yang et al., 2006; Wiley et al., 2007).

Co-expression of APP-Gal4 with the AICD-interacting protein Jip1b resulted in an approximately 70% decrease of the Cit signal as compared to Fe65 co-expression. Previous results have shown that Jip1b promotes AICD-mediated transcription differently from Fe65 (Scheinfeld et al., 2003). The reduced transcriptional activity is also in line with the observation that Jip1b localizes together with AICD predominantly to nuclear speckles and not to the spots associated with transcription (von Rotz et al., 2004; Konietzko et al., 2010). Co-expression of APP-Gal4 with the AICD-interacting protein Mint1, also known as X11, resulted in no increase of Cit signal as compared to expression of APP-Gal4 alone. The absent transcriptional activity is in line with the observation that Mint1 does not enter the nucleus and retains AICD in the cytosol (von Rotz et al., 2004; Riese et al., 2013). Likewise, in the original APP-Gal4 luciferase experiments as well as in experiments using chloramphenicol acetyl transferase reporters, Mint1 did not support APP-Gal4-mediated transcription (Cao and Sudhof, 2001; Zambrano et al., 2004). In summary, we observe that usage of the Gal4/UAS-Cit transcription assay recapitulates described properties of APP-binding proteins with respect to nuclear signaling.

Glycine 681 is a flexible linker in AICD that connects helix αN to the YENPTY motif (Radzimanowski et al.,

2008) and is essential for the interaction with Fe65 as mutation to alanine completely abolishes co-immunoprecipitation (Cao and Sudhof, 2004). G681A mutation in APP-Gal4 abolished the Cit signal, even with 1 µg of APP and Fe65 plasmids, which is in the saturated range of the assay with wild-type APP. Of note, the G681A mutant APP also resulted in strongly reduced mature APP levels, pointing to a role of Fe65 in APP maturation.

When expressing Fe65 that does not contain the Gal4-DBD without APP-Gal4 co-expression, we also could not detect a Cit signal. Thus, only when Gal4-AICD can bind Fe65 can direct it to the UAS elements to induce Cit expression. We have further observed that the position of the Gal4-DBD fusion strongly influences transcriptional activity. The formation of a transcriptionally active complex should not occlude the binding of the Gal4-DBD to the UAS elements and enable RNA polymerase II to be positioned correctly to initiate transcription. The dramatically reduced activity of the APP-Gal4ct construct, as compared to APP-Gal4, could be an occlusion of the C-terminal Gal4-DBD by Fe65, which has an extended interaction interface with the C-terminus of AICD (Radzimanowski et al., 2008). Alternatively, the position of the Gal4-DBD in APP might affect the rate of γ-secretase cleavage, leading to an increase in the case of insertion after the ε-cleavage site. We think this is unlikely, because expression of an AICD-Gal4ct construct together with Fe65 revealed only minor induction of Cit expression compared to APP-Gal4 with the internal Gal4-DBD (data not shown). We have reported that the N-terminal residues of AICD determine its turnover – replacing the stabilizing AICD VML sequence with LLR from the AL1ICD that is degraded at higher rates strongly reduced AICD levels (Gersbacher et al., 2013). Comparing an APP-Gal4 VML-LLR mutant with wild-type APP-Gal4, we saw a strong reduction in the Cit signal, both with confocal microscopy and plate reader analysis. The availability of Gal4-AICD thus controls Cit expression by Fe65. It was proposed that AICD is not necessary for Fe65 to translocate to the nucleus and regulate transcription (Cao and Sudhof, 2004). Gal4-AICD is necessary in the Gal4/UAS-Cit transcription assay, but this might be because of the artificial Gal4-DBD-UAS interaction. Promoters of endogenous target genes will be bound via a different mechanism by Fe65. With confocal microscopy, AICD can be seen co-localizing with Fe65 and Tip60 in nuclear AFT spots (von Rotz et al., 2004; Goodger et al., 2009). Fe65 dimerizes via its second phosphotyrosine-binding domain (PTB), and binding of AICD to the Fe65 PTB2 might be necessary to dissolve dimerization and enable interaction with Tip60 to target AFT spots to endogenous promoters of target genes (Konietzko et al., 2010).

Phosphorylation of proteins regulates their interaction with other proteins and is a major mechanism of signal transduction. We therefore studied the impact of APP phosphorylation sites on its nuclear signaling. All mutants were initially tested with 1-µg plasmid, which lies in the saturated range of the UAS-Cit assay and we could not detect any difference in the Cit signal compared to wild-type APP (data not shown) If phosphorylation only modifies signaling and has no on-off effect, such as the G681A mutation, which disrupts Fe65 binding, changes can only be detected in the linear range of the assay. We therefore analyzed transfections of 100-ng APP-Gal4 plasmids harboring the different mutations. S655 is part of the YTSI basolateral sorting signal in APP, and phosphorylation was shown to enhance secretory trafficking and decrease lysosomal targeting (Vieira et al., 2009; Vieira et al., 2010). In line with these data, the APP-Gal4 S655A mutant that cannot be phosphorylated reduced the Cit reporter signal in our assay. T668 has been extensively studied, with conflicting results of its phosphorylation resulting in increased or decreased Fe65 interaction (Ando et al., 2001; Chang et al., 2006). Analysis of T668A knock-in mice argued against a prominent role, as the mice did not show the expected deficits (Sano et al., 2006; Barbagallo et al., 2011). The APP-Gal4 T668A mutant showed a slightly increased induction of the Cit signal, which would be an indication for reduced Fe65 interaction upon T668 phosphorylation. S675 has also been shown to be targeted by phosphorylation and acts in concert with T668 phosphorylation in synaptic activity-regulated Aβ production (Lee et al., 2017). The APP-Gal4 S675A mutant showed a similar increase in the Cit signal as T668A; thus, in our hands, these two sites both have small but significant impact on Fe65-mediated AICD nuclear translocation.

PTB-containing proteins belong to different groups that are dependent or independent of tyrosine phosphorylation in the NPXY motif for efficient binding (Uhlik et al., 2005). Y682 phosphorylation is not required for Fe65 binding (Borg et al., 1996) or even reduces it (Tamayev et al., 2009; Zhou et al., 2009). Mutation of Y682 to glycine inhibits Fe65 binding and dramatically shifts APP processing to the non-amyloidogenic pathway in knock-in mice (Barbagallo et al., 2010). We mutated Y682 to phenylalanine, which blocks phosphorylation but does not disrupt Fe65 binding. Consistent with the negative influence of Y682 phosphorylation of Fe65 binding, the Y682F mutant showed increased transcription of Cit. Mutation of the second tyrosine in the YENPTY motif resulted in reduced activity in the Gal4/UAS-Cit transcription assay. This can be explained by the reduced half-life of full-length APP reported for the Y687F mutation (Rebelo et al., 2007), which is also evident in the low levels of this

mutant detected in Western blot analysis. When more APP is shuttled toward the lysosome, there is less available for nuclear signaling. The alteration in Cit transcription upon mutation of the studied residues also implies that they are under the control of phosphorylation in cells. We showed previously that nuclear translocation of endogenous AICD also occurs in primary neurons and is similarly reduced by γ-secretase inhibition (Goodger et al., 2009). However, future experiments will be required to validate the modulatory role of endogenous APP phosphorylation in context of nuclear translocation and signaling.

We have established a novel cellular assay for nuclear translocation. Studying nuclear signaling by APP, we show that the assay can detect on-off regulation of transcription as well as modulatory changes of signaling by phosphorylation. The lentiviral reporter can be inserted into many cell lines or even primary cells. The Gal4/UAS-Cit transcription assay enables the study of bona fide nuclear signaling in situ and will be of great utility for the scientific community interested in studying nuclear signaling and transcriptional regulation on the cellular level in a quantitative manner.

Materials and methods

DNA constructs

The pUKBK expression vectors and clones of HA-Fe65, HA-X11, and HA-Jip1b were previously described (von Rotz et al., 2004; Kohli et al., 2012). pSCTGal (1–93)-VP16 (Gal4-VP16) was obtained from Prof. Walter Schaffner (University of Zurich, Switzerland) and encodes the DBD of the yeast Gal4 protein (amino acids 1–93) fused to the C-terminal 78 amino acids of the activation domain of the VP16 protein of the herpes simplex virus (Sadowski et al., 1988). The APP-Gal4 construct was obtained from Prof. Thomas Südhof (Stanford University, USA) and encodes the 695-amino acid isoform of APP with an internal Gal4-DBD after the ε-cleavage site preceding the basolateral sorting signal of AICD (Cao and Sudhof, 2001). APPGal4(VML646LLR) was created by side-directed mutagenesis of the APP residues valine646, methione647, and leucine648 to leucine, leucine, and arginine within the APPGal4 construct. We further inserted the APPGal4 sequence in the third-generation pSicoR lentivirus backbone, which was obtained from Prof. Ueli Suter (ETH Zurich, Switzerland) (Ventura et al., 2004). pUKBK-C-APP-Gal4ct encodes APP (695-amino acid isoform of human APP) fused at its C-terminus to the Gal4-DBD. The sequence was assembled by PCR-driven overlap extension (Heckman and Pease, 2007), followed by transfer to the pUKBK-C backbone. pCCL-9×UAS-Cit encodes the fluorescence protein Cit (Griesbeck et al., 2001) under the control of a 9× repeat of the Gal4 upstream activating sequence (UAS) motif, followed by the adenovirus late promoter in a third-generation lentivirus backbone (pCCL) (Dull et al., 1998). pCCL-P-EGFP was obtained from Prof. Ueli Suter. The sequence was assembled by PCR-driven overlap extension on pGL4.35[luc2P/9×GAL4UAS/Hygro] (Promega; Madison, WI, USA) and a Cit-containing vector (von Rotz et al., 2004), followed by transfer to the pCCL backbone. pCCL-9×UAS-Cit-NLS was derived from pCCL-9×UAS-Cit by insertion of three SV40 nuclear localization sequences (NLS) to the C-terminus of the Cit fluorescent protein by PCR-driven overlap extension. The pECFP-Nuc plasmid (Takara; Kusatsu, Shiga, Japan) served as a template for the 3×NLS sequence. Site-directed mutagenesis of pECFP-Nuc was used to create Cer-NLS according to the published sequence (Rizzo et al., 2004). Exchange of single amino acids in the AICD of APP-Gal4-DBD sequence was achieved by PCR-driven overlap extension using sequence-verified APP clones with the respective mutations.

Cell culture, serial dilution, and lipofection

Human embryonic kidney cells (HEK293; DSMZ; Braunschweig, Niedersachsen, Germany) and Lenti-X cells (Takara; Kusatsu, Shiga, Japan) were cultured at 37°C and 5% CO_2 in Dulbecco's modified eagle medium (DMEM with glutamine and 4.5 g/l D-glucose; Thermo Fisher Scientific; Waltham, MA, USA), supplemented with 10% fetal bovine serum (FBS; Thermo Fisher Scientific; Waltham, MA, USA). For plate reader or microscopy experiments, HEK293 were grown in multiwell plastic plates or on 4 well-chamber glass slides (Falcon; Corning GmbH; Kaiserslautern, Rheinland-Pfalz, Germany), successively coated with poly-L-ornithine (50 µg/ml; Merck; Darmstadt, Hessen, Germany) and fibronectin (5 µg/ml; Merck; Darmstadt, Hessen, Germany).

Plasmid DNA concentration was measured on a Nanodrop 2000 (Thermo Fisher Scientific; Waltham, MA, USA), and 500 ng of undigested DNA was routinely analyzed on agarose gels to ensure identical quality, i.e. supercoiled status that affects lipofection efficiency. For transfection of adherent cells, Lipofectamine 2000 (Thermo Fisher Scientific; Waltham, MA, USA) was used according to the manufacturer's protocol. The medium was replaced after 3 h and cells were fixed with 4% (w/v) paraformaldehyde 20–22 h after transfection. Nuclei were stained with DAPI (Merck; Darmstadt, Hessen, Germany). HA-tagged constructs were stained with anti-HA high affinity antibodies (Merck; Darmstadt, Hessen, Germany), followed by anti-rat secondary antibodies labeled with Alexa647 (Jackson Immunoresearch; Ely, Cambridge, UK).

Pharmacological inhibition of γ-secretase

To inhibit γ-secretase, DAPT (Merck; Darmstadt, Hessen, Germany) was added to the medium after transfection. 8×10^6 trypsinized (Gibco) cells in 2 ml medium were lipofected with 600 µl Opti-MEM (Thermo Fisher Scientific; Waltham, MA, USA) containing 3 µg DNA of each clone and 15 µl Lipofectamine 2000. The suspension was incubated for 1 h at 37°C with mild resuspension every 10 min. Cells were centrifuged, supernatant removed, resuspended in DMEM/FBS, cell numbers remeasured, and 3×10^5 cells plated per well on a 48-well plate. We performed square- and third-root serial dilutions of DAPT and DNA constructs, ensuring equidistance of data points on a logarithmic scale. To minimize variability of lipofection for different DNA concentrations, we added empty expression plasmids to fill-up the DNA to 1 µg. To control DAPT from causing cell death at higher concentrations, we performed colorimetric MTT assays (Merck; Darmstadt, Hessen, Germany) according to the manufacturer's protocol.

Virus production and cell line generation

Lenti-X cells were transfected with pCCL-9×UAS-Cit or pCCL-9×UAS-Cit-NLS, together with helper plasmids, by calcium phosphate transfection as described previously (Birnbaum et al., 2018). Virus-containing supernatant was sterile filtered and stored at −80°C until use. For generating the HEK:UAS-Cit cell line, 10^5 HEK293 cells were plated and infected the following day with 0.5 ml 9×UAS-Cit virus supernatant. Further, 10^5 HEK293 cells were plated and infected the following day with 1.2 ml 9×UAS-Cit-NLS virus supernatant yielding the cell line HEK1:UAS-Cit-NLS; 10^5 cells of this line were again infected with 1.2 ml virus supernatant generating line HEK2:UAS-Cit-NLS.

Western blotting

Cells were lyzed with RIPA buffer and lysates separated on Novex™ 16% Tricine Gels (Thermo Fisher Scientific; Waltham, MA, USA). After transfer to 0.1 µm Amersham™ Protran™ membranes (GE Healthcare; Chicago, IL, USA), the blots were probed with anti-APP antibody Y188 (ab32136; Abcam; Cambridge, Cambridge, UK), anti-GAPDH (H86504M; Milan Analytica AG; Rheinfelden, Aargau, Switzerland) and anti-HA high affinity (11867423001; Roche; Basel, Basel-Stadt, Switzerland), followed by peroxidase-linked secondary antibodies (Jackson Immunoresearch; Ely, Cambridge, UK). ECL detection was performed with the ImageQuant LAS 4000 (GE Healthcare; Chicago, IL, USA) using Pierce™ ECL Western Blotting Substrate (Thermo Fisher Scientific; Waltham, MA, USA) or ECL Prime Western Blotting Detection Reagent (GE Healthcare; Chicago, IL, USA).

Plate reader analysis

Multi-well plates were analyzed with a SPARK 10 M Multimode Reader (Tecan; Männedorf, Zürich, Switzerland). Cit fluorescence was imaged with a 485/20 nm excitation and a 535/35 nm emission filter (10 flashes, 7×7 reads per well of 48 wells or 10×10 for 24 wells). We used the 4× objective of the SPARK reader with bright-field illumination to determine cell confluence. The mean value of Cit fluorescence per well was normalized to cell confluence. Reporter cell lines without lipofection were plated in 3–6 wells to determine the limit of blank (LoB) = $\text{mean}_{\text{blank}} + 1.645\ (\text{SD}_{\text{blank}})$ (Armbruster and Pry, 2008). The LoB was subtracted from normalized Cit values, and values from experiments performed on different days with different cell passage numbers were normalized by sum division for comparison as described (Degasperi et al., 2014).

Confocal microscopy

Images were acquired on a TCS/SP8 confocal microscope (Leica; Wetzlar, Hessen, Germany) with a 20× glycerol objective. Hybrid detectors (HyDs) were operated in count mode with 12-bit intensity resolution. DAPI was excited with a 405-nm diode laser and detected with a HyD window of 407–507 nm. Cit was excited with the 514-nm line of the argon laser and detected with a HyD window of 516–625 nm. Cer was excited with the 458-nm line of the argon laser and detected with a HyD window of 460–510 nm. In this case, the HyD window for DAPI was set from 407 to 456 nm to prevent signal pickup from Cer. Alexa647 was excited with a 633-nm helium-neon laser and detected with a HyD window of 635–740 nm. For every experiment, we initially scanned all conditions in the Cit channel visually via the ocular, to determine the brightest Cit fluorescence. With this condition, we adjusted laser intensity and accumulation number to avoid saturating the HyDs. We adjusted the z-position to achieve the brightest DAPI signal and acquired 5–7 images per condition (frame 775×775 µm; ~2000 cells). This way, the Cit channel is imaged for the first time during actual acquisition, preventing any bias or bleaching.

Image analysis

All image analysis was performed using Fiji/ImageJ (NIH; Bethesda, MD, USA). To determine the strength of transcriptional activation, we measured Cit or Cer integrated density (mean intensity×area) either over the whole frame for Cit or solely in the nucleus for Cit-NLS and Cer-NLS. Integrated density values were normalized by the number of DAPI-stained nuclei. First, a threshold that detects nearly all nuclei was selected for the DAPI channel. Then, the image was converted to mask, and the nuclei were separated using the watershed algorithm. The particle analyzer was applied to obtain the DAPI outlines with a size between 60 and 230 μm^2, thus excluding small mitotic DAPI profiles, for example. For transactivation assays using the Cit readout, the total Cit/DAPI was calculated by dividing the integrated Cit over the whole image frame by the number of DAPI counts. The NLS-tagged fluorescent proteins are targeted to the nucleus and the integrated densities of the Cit-NLS or CER-NLS fluorescence in the DAPI outlines were measured, followed by dividing the sum of the integrated Cit or Cer densities by the number of DAPI counts. HA-tagged proteins were stained with anti-HA high-affinity antibody (11867423001; Roche; Basel, Basel-Stadt, Switzerland) and Alexa647-labeled anti-rat antibody (Jackson Immunoresearch; Ely, Cambridge, UK), followed by the measurement of total fluorescence and normalization to DAPI counts. Data from Fiji were transferred to Excel or Prism for further analysis.

Statistical analysis

Statistics were calculated with Prism 6 (Graph Pad; San Diego, CA, USA). Data were controlled for normal distribution and analyzed by Student's *t*-test against control or wild type. Asterisks above the horizontal significance line refers to all bars with ticks except when the ticks are marked individually (*$p < 0.05$, **$p < 0.01$, and ***$p < 0.001$). Bars not marked by a tick are not significantly different. Data are presented with average values and standard deviation (SD).

Acknowledgments: We thank Roger Frei (Tecan, Switzerland) for his support with setting up the Tecan reader measurements. We are grateful to all scientists that supplied us with constructs as mentioned under methods. This work was supported by the Swiss National Science Foundation SNF Funder Id: http://dx.doi.org/10.13039/501100001711, Grant Number: 31003A_166177.

Conflict of interest statement: None to declare.

References

Ando, K., Iijima, K.I., Elliott, J.I., Kirino, Y., and Suzuki, T. (2001). Phosphorylation-dependent regulation of the interaction of amyloid precursor protein with Fe65 affects the production of beta-amyloid. J. Biol. Chem. *276*, 40353–40361.

Armbruster, D.A. and Pry, T. (2008). Limit of blank, limit of detection and limit of quantitation. Clin. Biochem. Rev. *29*(Suppl. 1), S49–52.

Bai, H., Lester, G.M.S., Petishnok, L.C., and Dean, D.A. (2017). Cytoplasmic transport and nuclear import of plasmid DNA. Biosci. Rep. *37*, 1–17.

Barbagallo, A.P., Weldon, R., Tamayev, R., Zhou, D., Giliberto, L., Foreman, O., and D'Adamio, L. (2010). Tyr(682) in the intracellular domain of APP regulates amyloidogenic APP processing in vivo. PLoS One *5*, e15503.

Barbagallo, A.P., Wang, Z., Zheng, H., and D'Adamio, L. (2011). The intracellular threonine of amyloid precursor protein that is essential for docking of pin1 is dispensable for developmental function. PLoS One *6*, e18006.

Birnbaum, J.H., Wanner, D., Gietl, A.F., Saake, A., Kundig, T.M., Hock, C., Nitsch, R.M., and Tackenberg, C. (2018). Oxidative stress and altered mitochondrial protein expression in the absence of amyloid-beta and tau pathology in iPSC-derived neurons from sporadic Alzheimer's disease patients. Stem Cell Res. *27*, 121–130.

Borg, J.P., Ooi, J., Levy, E., and Margolis, B. (1996). The phosphotyrosine interaction domains of X11 and FE65 bind to distinct sites on the YENPTY motif of amyloid precursor protein. Mol. Cell Biol. *16*, 6229–6241.

Borg, J.P., Yang, Y., De Taddeo-Borg, M., Margolis, B., and Turner, R.S. (1998). The X11alpha protein slows cellular amyloid precursor protein processing and reduces Abeta40 and Abeta42 secretion. J. Biol. Chem. *273*, 14761–14766.

Cao, X. and Sudhof, T.C. (2001). A transcriptionally [correction of transcriptively] active complex of APP with Fe65 and histone acetyltransferase Tip60. Science *293*, 115–120.

Cao, X. and Sudhof, T.C. (2004). Dissection of amyloid-beta precursor protein-dependent transcriptional transactivation. J. Biol. Chem. *279*, 24601–24611.

Chang, K.A., Kim, H.S., Ha, T.Y., Ha, J.W., Shin, K.Y., Jeong, Y.H., Lee, J.P., Park, C.H., Kim, S., Baik, T.K., et al. (2006). Phosphorylation of amyloid precursor protein (APP) at Thr668 regulates the nuclear translocation of the APP intracellular domain and induces neurodegeneration. Mol. Cell Biol. *26*, 4327–4338.

Cho, W.K., Spille, J.H., Hecht, M., Lee, C., Li, C., Grube, V., and Cisse, I.I. (2018). Mediator and RNA polymerase II clusters associate in transcription-dependent condensates. Science *361*, 412–415.

De Strooper, B. and Annaert, W. (2000). Proteolytic processing and cell biological functions of the amyloid precursor protein. J. Cell Sci. *113*(Pt 11), 1857–1870.

De Strooper, B., Annaert, W., Cupers, P., Saftig, P., Craessaerts, K., Mumm, J.S., Schroeter, E.H., Schrijvers, V., Wolfe, M.S., Ray, W.J., et al. (1999). A presenilin-1-dependent gamma-secretase-like protease mediates release of Notch intracellular domain. Nature *398*, 518–522.

Degasperi, A., Birtwistle, M.R., Volinsky, N., Rauch, J., Kolch, W., and Kholodenko, B.N. (2014). Evaluating strategies to normalise biological replicates of Western blot data. PLoS One *9*, e87293.

Dovey, H.F., John, V., Anderson, J.P., Chen, L.Z., de Saint Andrieu, P., Fang, L.Y., Freedman, S.B., Folmer, B., Goldbach, E., Holsztynska, E.J., et al. (2001). Functional gamma-secretase inhibitors reduce beta-amyloid peptide levels in brain. J. Neurochem. *76*, 173–181.

Duffy, J.B. (2002). GAL4 system in Drosophila: a fly geneticist's Swiss army knife. Genesis *34*, 1–15.

Duilio, A., Zambrano, N., Mogavero, A.R., Ammendola, R., Cimino, F., and Russo, T. (1991). A rat brain mRNA encoding a transcriptional activator homologous to the DNA binding domain of retroviral integrases. Nucleic Acids Res. *19*, 5269–5274.

Dull, T., Zufferey, R., Kelly, M., Mandel, R.J., Nguyen, M., Trono, D., and Naldini, L. (1998). A third-generation lentivirus vector with a conditional packaging system. J. Virol. *72*, 8463–8471.

Gersbacher, M.T., Goodger, Z.V., Trutzel, A., Bundschuh, D., Nitsch, R.M., and Konietzko, U. (2013). Turnover of amyloid precursor protein family members determines their nuclear signaling capability. PLoS One *8*, e69363.

Goodger, Z.V., Rajendran, L., Trutzel, A., Kohli, B.M., Nitsch, R.M., and Konietzko, U. (2009). Nuclear signaling by the APP intracellular domain occurs predominantly through the amyloidogenic processing pathway. J. Cell Sci. *122*, 3703–3714.

Griesbeck, O., Baird, G.S., Campbell, R.E., Zacharias, D.A., and Tsien, R.Y. (2001). Reducing the environmental sensitivity of yellow fluorescent protein. Mechanism and applications. J. Biol. Chem. *276*, 29188–29194.

Heckman, K.L. and Pease, L.R. (2007). Gene splicing and mutagenesis by PCR-driven overlap extension. Nat. Protoc. *2*, 924–932.

Kakidani, H. and Ptashne, M. (1988). GAL4 activates gene expression in mammalian cells. Cell *52*, 161–167.

Kimberly, W.T., Zheng, J.B., Guenette, S.Y., and Selkoe, D.J. (2001). The intracellular domain of the beta-amyloid precursor protein is stabilized by Fe65 and translocates to the nucleus in a notch-like manner. J. Biol. Chem. *276*, 40288–40292.

Kohli, B.M., Pflieger, D., Mueller, L.N., Carbonetti, G., Aebersold, R., Nitsch, R.M., and Konietzko, U. (2012). Interactome of the amyloid precursor protein APP in brain reveals a protein network involved in synaptic vesicle turnover and a close association with synaptotagmin-1. J. Proteome Res. *11*, 4075–4090.

Konietzko, U., Goodger, Z.V., Meyer, M., Kohli, B.M., Bosset, J., Lahiri, D.K., and Nitsch, R.M. (2010). Co-localization of the amyloid precursor protein and Notch intracellular domains in nuclear transcription factories. Neurobiol. Aging *31*, 58–73.

Lee, Y., Lee, J.S., Lee, K.J., Turner, R.S., Hoe, H.S., and Pak, D.T.S. (2017). Polo-like kinase 2 phosphorylation of amyloid precursor protein regulates activity-dependent amyloidogenic processing. Neuropharmacology *117*, 387–400.

Muller, T., Concannon, C.G., Ward, M.W., Walsh, C.M., Tirniceriu, A.L., Tribl, F., Kogel, D., Prehn, J.H., and Egensperger, R. (2007). Modulation of gene expression and cytoskeletal dynamics by the amyloid precursor protein intracellular domain (AICD). Mol. Biol. Cell *18*, 201–210.

Pardossi-Piquard, R. and Checler, F. (2012). The physiology of the beta-amyloid precursor protein intracellular domain AICD. J. Neurochem. *120*(Suppl 1), 109–124.

Radzimanowski, J., Simon, B., Sattler, M., Beyreuther, K., Sinning, I., and Wild, K. (2008). Structure of the intracellular domain of the amyloid precursor protein in complex with Fe65-PTB2. EMBO Rep. *9*, 1134–1140.

Rebelo, S., Vieira, S.I., Esselmann, H., Wiltfang, J., da Cruz e Silva, E.F., and da Cruz e Silva, O.A. (2007). Tyrosine 687 phosphorylated Alzheimer's amyloid precursor protein is

retained intracellularly and exhibits a decreased turnover rate. Neurodegener Dis. *4*, 78–87.

Riese, F., Grinschgl, S., Gersbacher, M.T., Russi, N., Hock, C., Nitsch, R.M., and Konietzko, U. (2013). Visualization and quantification of APP intracellular domain-mediated nuclear signaling by bimolecular fluorescence complementation. PLoS One *8*, e76094.

Rizzo, M.A., Springer, G.H., Granada, B., and Piston, D.W. (2004). An improved cyan fluorescent protein variant useful for FRET. Nat. Biotechnol. *22*, 445–449.

Sabo, S.L., Lanier, L.M., Ikin, A.F., Khorkova, O., Sahasrabudhe, S., Greengard, P., and Buxbaum, J.D. (1999). Regulation of beta-amyloid secretion by FE65, an amyloid protein precursor-binding protein. J. Biol. Chem. *274*, 7952–7957.

Sadowski, I., Ma, J., Triezenberg, S., and Ptashne, M. (1988). GAL4-VP16 is an unusually potent transcriptional activator. Nature *335*, 563–564.

Sano, Y., Nakaya, T., Pedrini, S., Takeda, S., Iijima-Ando, K., Iijima, K., Mathews, P.M., Itohara, S., Gandy, S., and Suzuki, T. (2006). Physiological mouse brain Abeta levels are not related to the phosphorylation state of threonine-668 of Alzheimer's APP. PLoS One *1*, e51.

Scheinfeld, M.H., Matsuda, S., and D'Adamio, L. (2003). JNK-interacting protein-1 promotes transcription of A beta protein precursor but not A beta precursor-like proteins, mechanistically different than Fe65. Proc. Natl. Acad. Sci. U.S.A. *100*, 1729–1734.

Scott, E.K. (2009). The Gal4/UAS toolbox in zebrafish: new approaches for defining behavioral circuits. J. Neurochem. *110*, 441–456.

Tamayev, R., Zhou, D., and D'Adamio, L. (2009). The interactome of the amyloid beta precursor protein family members is shaped by phosphorylation of their intracellular domains. Mol. Neurodegener. *4*, 28.

Taru, H., Kirino, Y., and Suzuki, T. (2002). Differential roles of JIP scaffold proteins in the modulation of amyloid precursor protein metabolism. J. Biol. Chem. *277*, 27567–27574.

Uhlik, M.T., Temple, B., Bencharit, S., Kimple, A.J., Siderovski, D.P., and Johnson, G.L. (2005). Structural and evolutionary division of phosphotyrosine binding (PTB) domains. J. Mol. Biol. *345*, 1–20.

Ventura, A., Meissner, A., Dillon, C.P., McManus, M., Sharp, P.A., Van Parijs, L., Jaenisch, R., and Jacks, T. (2004). Cre-lox-regulated conditional RNA interference from transgenes. Proc. Natl. Acad. Sci. U.S.A. *101*, 10380–10385.

Vieira, S.I., Rebelo, S., Domingues, S.C., da Cruz e Silva, E.F., and da Cruz e Silva, O.A. (2009). S655 phosphorylation enhances APP secretory traffic. Mol. Cell. Biochem. *328*, 145–154.

Vieira, S.I., Rebelo, S., Esselmann, H., Wiltfang, J., Lah, J., Lane, R., Small, S.A., Gandy, S., da Cruz, E.S.E.F., and da Cruz, E.S.O.A. (2010). Retrieval of the Alzheimer's amyloid precursor protein from the endosome to the TGN is S655 phosphorylation state-dependent and retromer-mediated. Mol. Neurodegener *5*, 40.

von Rotz, R.C., Kohli, B.M., Bosset, J., Meier, M., Suzuki, T., Nitsch, R.M., and Konietzko, U. (2004). The APP intracellular domain forms nuclear multiprotein complexes and regulates the transcription of its own precursor. J. Cell Sci. *117*, 4435–4448.

Wiley, J.C., Smith, E.A., Hudson, M.P., Ladiges, W.C., and Bothwell, M. (2007). Fe65 stimulates proteolytic liberation of the beta-amyloid precursor protein intracellular domain. J. Biol. Chem. *282*, 33313–33325.

Yang, Z., Cool, B.H., Martin, G.M., and Hu, Q. (2006). A dominant role for FE65 (APBB1) in nuclear signaling. J. Biol. Chem. *281*, 4207–4214.

Zambrano, N., Gianni, D., Bruni, P., Passaro, F., Telese, F., and Russo, T. (2004). Fe65 is not involved in the platelet-derived growth factor-induced processing of Alzheimer's amyloid precursor protein, which activates its caspase-directed cleavage. J. Biol. Chem. *279*, 16161–16169.

Zhou, D., Zambrano, N., Russo, T., and D'Adamio, L. (2009). Phosphorylation of a tyrosine in the amyloid-beta protein precursor intracellular domain inhibits Fe65 binding and signaling. J. Alzheimers Dis. *16*, 301–307.